Particle Motion and Deposition near Multifluid Interfaces

by Leo(Tsung-Cheng) Feng

A dissertation submitted to Johns Hopkins University in conformity with the requirements for the degree of Master of Science in Chemical & Biomolecular Engineering

Johns Hopkins University

Baltimore, MD 21218

June 2017

ABSTRACT

Particle motion and deposition near multifluid interface (June, 2017)

Tsung-Cheng Feng, B.S., Johns Hopkins University, USA

Chair of Advisory Committee: Dr. Joelle Frechette & Dr. Michael A. Bevan

Studying particle motion and deposition near different fluid interfaces are important to understand not only to separate species of interest for diagnostics but also to hierarchically assemble nanomaterials for continuous nanomanufacturing practices. My master thesis covers two aspects of particle interactions with different interfaces. The first half of my research compares the interfacial effect of solid and fluid interfaces to particles trajectory motions for single obstacle separation microscopically. We observe a clear particle separation theme for both solid and fluid obstacles in a gravity driven flow. The second half of my research focuses on constructing a chemically pre-defined surface for oil drop with nanoparticles(Nps) deposition in situ polymerizable medium to form hierarchical nanomaterials. We successfully create a heterogenous patterned surface for ETPTA oil with nanoparticle drop to be deposited and confined at pre-defined regions. Using external magnetic field, we hope to alter the configuration of particles within drops. Finally, we capture local and global nanostructures in situ polymerizable ETPTA oil medium. Understanding fundamental interfacial phenomena and apply the knowledge to study particle motion or particle deposition in multifluid interfaces allow us to create more robust device for particle separation and utilizing knowledge of surface characterization to construct more tunable hierarchical nanomaterials.

To my Mom and Dad

ACKNOWLEDGEMENTS

I would like to thank my parents for supporting me to finish BS/MSE in Chemical & Biomolecular Engineering at Johns Hopkins University. I will not have done so without their love and guidance. I want to thank my advisor, Dr. Joelle Frechette, for motivating my passion for research.

Specifically, I would like to acknowledge Tianyu Yan, a former master student at Frechette lab now a PhD student at Penn State University for the support and collaboration on the first half of my research. We together conducted particle separation experiments, analyzed data sets and had meaningful discussion (we shared some of the data analysis graphs and experimental data). Without her help, I will not have finished the project by myself along the guidance of Dr. German Drazer and Siqi Du, a PhD student at Rutgers, the state university of New Jersey.

Moreover, I would like to acknowledge Dr. Xue Li, a former post-doc at Bevan Lab for sharing her early investigation and research knowledge on the hierarchical nanomaterial project.

Finally, I want to thank all the members in both Dr. Frechette and Bevan's Lab for helping me learn different research techniques.

TABLE OF CONTENTS

LIST OF FIGURES

LIST OF TABLES

1. Particle motion near fluid interface

1.1 Introduction

The development of microfluidic separation technology is based on the quest to separate chemical or biological species of interest with higher throughput, sensitivity and efficiency. The applications can be found in many medical tests, biochemical essays, chemical processing and environmental assessments[1,2]. One advantage of microfluidic separation technique is that a small sample volume is required for less cost in reagent, device fabrication and continuous operation. Hydrodynamic separation in microfluidic devices depicts the behavior of the particles near obstacle with a restriction[3,4]. The interaction also provides a simple model to mimic numerous phenomenon in micro- or macroscale, including emulsions, flotation, and transport in porous media[5–7]. We developed a simple yet versatile microfluidic platform employing semi-circular cylinder solid (PDMS) and fluid (bubble) obstacle in PDMS microchannel, to imitate the colloidal transport on solid-water (SWI) and air-water (AWI) in subsurface. At first we employ pressure-driven flow to drive the particles in the microchannel. While particles moving downstream to interact with fluid interface or PDMS solid obstacle, particles never stick onto either AWI or SWI, but rather move around the obstacle. Then we utilize gravity to drive the particles through the channel by tilting microscopes. Here we observe both symmetric and asymmetric particle trajectories.

1.2 Material & Methods

Elastomer (Dow Corning Sylgard 184) is purchased from Robert McKeown Inc. (Branchburg, NJ). Silicon wafer is purchased from University Wafer (Boston, MA). SU-8 2025 and SU-8 2075 photoresist and developer are purchased from Microchem Corp.

(Newton, MA). Coverslips（12-545-J 22×60–1) purchased from Thermo Fisher Scientific Inc. (Pittsburg, PA). Sodium Dodecyl Sulfate (SDS) is purchased from Sigma-Aldrich (St. Louis, MO) and diluted with deionized water to a final concentration of 5mM. Silica particles (diameter = 10, 15, 20μm) are purchased from Bang's Laboratories (Fishers, IN) and sulfate polystyrene latex particles (diameter = 3, 5, 9, 20μm) are purchased from Thermo Fisher Scientific Inc. (Pittsburg, PA). Unless mentioned otherwise, all chemicals are used as received.

1.2.1 Microfabrication

In order to compare the difference between fluid and solid interface, two types of microfluidics channel were fabricated by standard soft photolithography[8,9] process. Micropatterns, which serve as template for the microfluidic channels, are fabricated on a silicon wafer to reach a final thickness of either 33μm (SU-8 2025) or 100μm (SU-8 2075). The elastomer base and curing agent are mixed in a 10:1 ratio and then spin-coated onto the mold, followed by degassing under vacuum for 20 minutes. The degassed elastomer is then place in 70 °C oven overnight. The cured substrate is peeled off from the mold. Both inlets and outlet are punched using a 0.75 mm Uni-core biopsy puncher (Harris, Ted Pella, Inc. USA). The microchannel and coverslips are then treated with oxygen plasma (Technics PEII A/B) and bonded with one another.

Two different microfluidic devices are fabricated. First, a standard T-channel[10] is employed to study the particle trajectories around a captive fluid obstacle (Figure 1A). Second, a channel with a cylindrical obstacle is fabricated to study particle trajectories around a solid obstacle (Figure 1B). All the channels have rectangular cross-sections. Dimensions of the channels are listed in Table 1.

1.2.2 Surface Characterization

An optical 3D laser scanning microscope (Keyence VK–X100) is used to measure the final dimensions of the microchannel shown in Figure 1 and in Table 1.

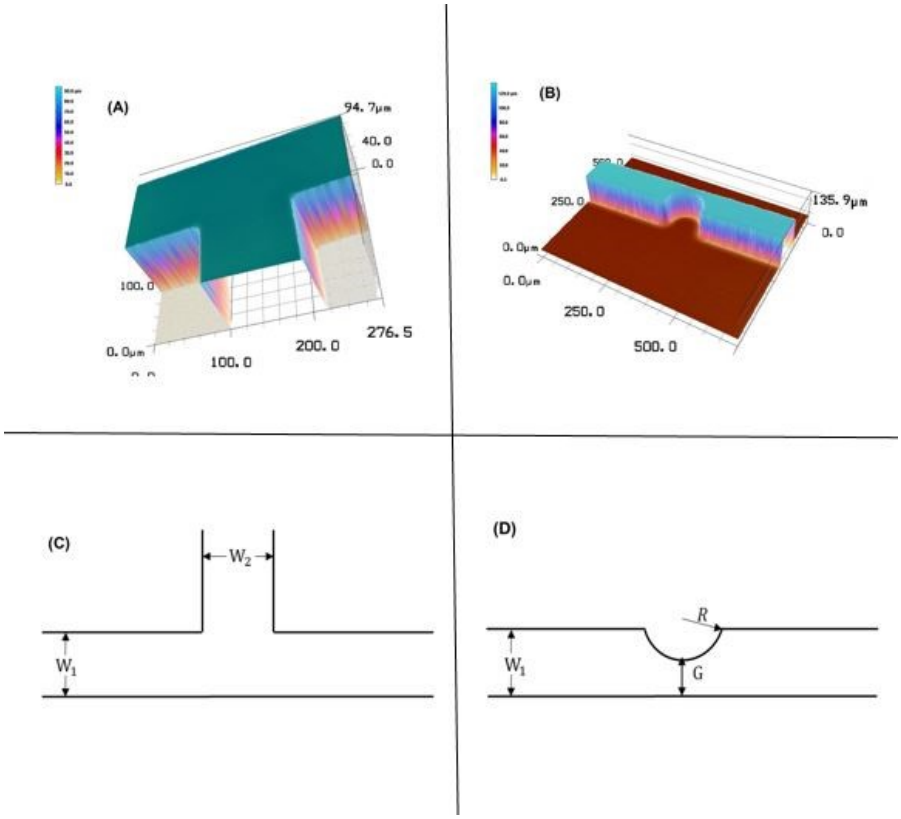

Figure 1. 3D optical microscopic image of (A) T–channel and (B) microchannel with a half-hemisphere solid obstacle. Schematic illustration of (C) T–channel and (D) microchannel with a half-hemisphere solid obstacle. The dimension of microchannel are shown in Table 1.

Table 2. Dimensions of microchannel

Model	Width W_1 (μm)	Width W_2 (μm)	Height H (μm)	Obstacle Radius R (μm)	Gap G (μm)
T-Channel	100	100	100	20-40	40
Regular-Channel	100	-	100	60	40

Sulfate polystyrene(PS) latex particles are dispersed in a 5mM aqueous sodium dodecyl sulfate (SDS) solutions to a final concentration of approximately 0.4% (w/v) while silica particles are dispersed in deionized water to a final concentration of approximately 0.2% (w/v), followed by sonication for two minutes before each experiment. We flow PS particle solution in the horizontal channel and pump air downwards in the vertical channel to create a bubble fluid interface right at the T junction. By adjusting the pressure difference from all three inlets, we can control and change the bubble sizes and flow rates. Images are captured by Nikon Confocal microscope and are processed by NIS Elements Viewer software. The air bubble and the flow of the polystyrene particle solution are controlled by a pressure system. Pressure difference between the inlet and outlet of the T-channel ranged from 0.1-0.3psi, giving a flow rate of approximately 200μm/s. Silica particle solution is injected into channel using a Hamilton Syringe to pump in air column. The device is leveled on the microscope. The silica particles were driven by gravity when tilting the entire microscope at about 15° to 20°. The Images were captured using MC352+ microscope and were processed by Motic image software. We also utilize COMSOL Multiphysics 5.1 to model our single fluid flow with stokes flow assuming incompressible flow and no slip boundary condition with the channel wall. Then by selecting stationary for time independent calculation and

setting up pressure different between inlet and outlet, we will get the velocity distribution that is comparable to our experimental setup shown in Figure 2.

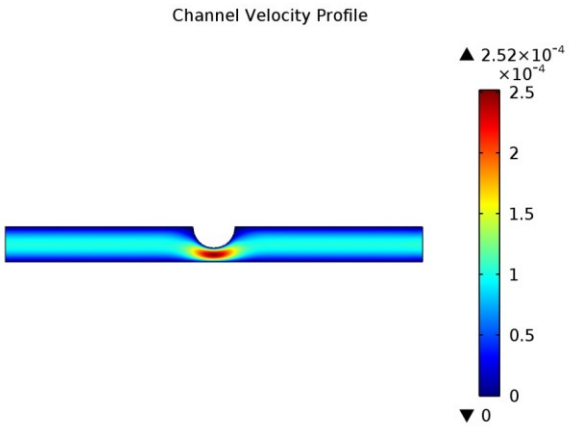

Figure 2. COMSOL velocity distribution across microfluidic channel

1.3 Result & Discussion

1.3.1 Determination of critical impact parameter

We employ the simple particle-obstacle model[11] to describe the trajectories of particles interacting around fixed sphere solid and fluid obstacles. We hypothesize that in such particle-obstacles collision particles may experience irreversible interaction that leads to a net lateral displacement for both occasions. The hypothesis of the simple model we used here is analogous to those used to describe force driven DLD systems (More detailed discussions can be found elsewhere[111213]). In this model, there are two main events depicting particle-obstacle planar collision. The first such event is illustrated with the blue trajectory line in Figure 3A. as purely hydrodynamics interaction between particles and the obstacle. The resulting symmetric trajectories of the particles past around the obstacle also gives rise to reversibility[14]. The second event is a particle–obstacle collision where particles

collide with the obstacle shown in the red and yellow trajectories. This touching collision demonstrated the solid-solid short ranged repulsive non-hydrodynamic forces as the underlying mechanism leading to irreversibility[15]. We analyzed particle position data as well as constructing particle trajectories data by utilizing three important parameters in the simple model. First, the incoming offset, b_{in} , is defined as the vertical distance between the asymptotic line of particle trajectory and the obstacle center before the collision illustrated in Figure 3. Second, we characterize the outgoing offset, b_{out}, as the vertical distance between the asymptotic line of particle trajectory and the obstacle center after the collision. Third, a critical value defined as b_c, is a critical collision impact factor that serves as a benchmark for differentiating two types of interaction/collision in our system. When $b_{in} > b_c$, the particle trajectory passing around the obstacle becomes symmetric as predicted from the Stokes flow (referred to the top trajectory in Figure 3). In other words, the interaction is purely hydrodynamic with $b_{in} = b_{out}$. We conclude that there is a reversible collision. In contrast, if $b_{in} < b_c$ shown in the yellow trajectory in Figure 8, the interaction is an irreversible one with their outgoing offset $b_c = b_{out}$, indicating a net lateral displacement of magnitude $(b_c - b_{in})$. In fact, experimentally for every incoming particle with $b_{in} < b_c$, a collapse of irreversible trajectories after the collision will be observed, converging into a single post-interaction particle trajectory (shown in the collapse of yellow and red trajectories). The resulting b_c represent an evidence of particle separation down in micron-scale. Different particles when interacting with obstacles would give different values of b_c for different level of separation. Thus, given particle size and its properties, we can deduce its b_c to be the fundamental theory basis to achieve and engineer desirable particle separation scheme.

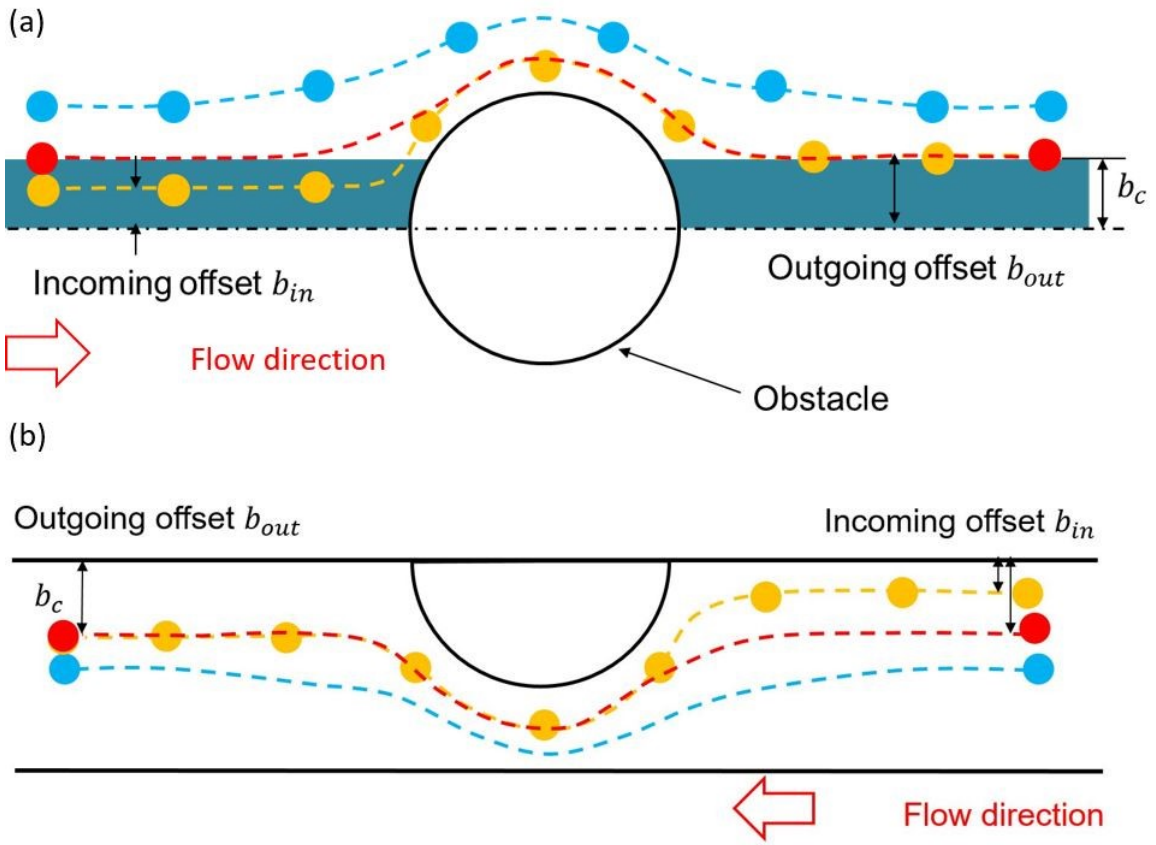

Figure 3. (a)Schematic illustration of reversible and irreversible particle trajectories around a fixed sphere obstacle in particle–obstacle collision simple model. The symmetric trajectory on top shows reversible, purely hydrodynamic collisions where $b_{in} > b_c$ and $b_{in} = b_{out}$. The asymmetric trajectory on bottom shows irreversible, touching collisions where $b_{in} < b_c$ and $b_{out} = b_c$. (b) Our experimental setup with simple model collision illustration

1.3.2 Particle trajectories under pressure-driven flow

Solutions with dispersed polystyrene particles are injected into the horizontal channel of a T-shaped microfluidic device. The trajectories of the particles are monitored as particle of interest flow past the solid or bubble obstacle under pressure-driven flow. We monitor both the incoming and outgoing offsets b_{in} and b_{out}. We find that, under pressure-driven flow, the particle trajectories are always symmetric for both solid and fluid obstacles as shown in Figure 4. All data points fall onto the asymptotic line ($b_{in} = b_{out}$, with slope

=1). The exception we observe is in the case of the fluid obstacle when the diameter of the particle is comparable to the minimum gap at the constriction. Specifically, we observe that $b_{out} < b_{in}$, which suggests that particles might have gone above or below the center point of the bubble where the radius of the bubble is the greatest. The meniscus of AWI is not perfectly cylindrical, due in part to pinning of the contact line at the upper and lower surfaces of the microfluidic device. The shape distortion of the meniscus allows particles to move at the z-direction while particles navigating through a highly pinched constriction. This particular experimental observation of fluid pinched effect is similar to that of pinched flow fractionation in microfluidic device.[14] In all other instances the trajectories are symmetric across the fluid flow channel.

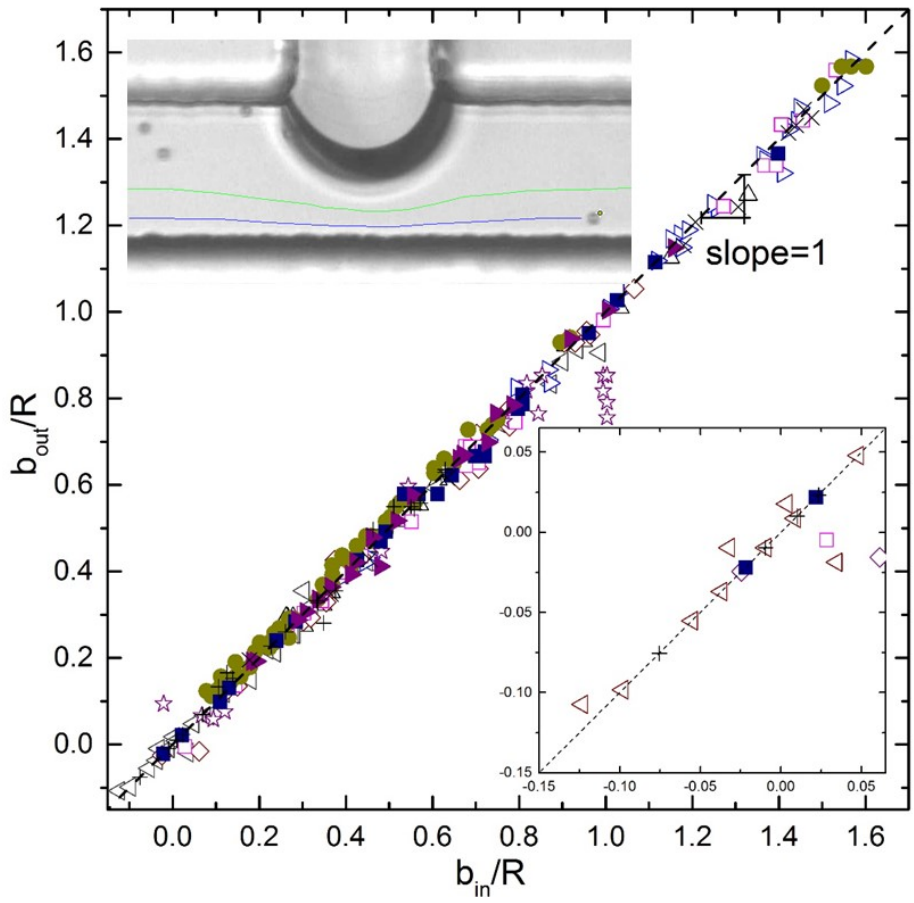

Figure 4. Outgoing offset ($\boldsymbol{b_{out}}$) as a function of the incoming offset ($\boldsymbol{b_{in}}$), both normalized by the obstacle radius (R) for polystyrene particles in pressure-driven flow. Here all solid symbols indicate trajectories for the solid obstacle while hollow symbols indicate trajectories for the fluid obstacle. The inset illustrates the incoming and outgoing offsets of the particles that interact with non-cylindrical part of the obstacle. The dash line illustrates the linear trend of "bin=bout". Different gap size (G in μm), channel heights(H) and particle radius (a in μm) in the figure are (△), H=100, G=4.4, a=1.5; (▽), H=100, G=31.2, a=1.5; (◁) , H=100 , G=13, a=2.5; (▷), H=100, G=13, a=2.5; (◇), H=100, G=30,a=4.5; (□) ,H=100, G=10,a=4.5; (☆), H=100, G=6,a=10; (●), H=100, G=40,a=4.5; (■), H=100, G=30,a=4.5; (►), H=100, G=20,a=4.5; (+), H=33 G=47, a=1.5; (×), H=33, G=113, a=2.5

However, our experimental result is in contrast with previous research findings where the presence of critical offset b_c has been commonly observed in pressure driven DLD systems[14,13,16]. The collision model also theoretically predicted that in a flow driven

environment the irreversible collision exists in a particle-obstacle (solid) interaction [4]. Asymmetric is observed when particles when the particle comes to a particle-obstacle collision with $b_{in} < b_c$ in a pressure driven fluid flow.

One explanation accounted for the difference between our experimental results and in previous related work is the restriction of the top wall in the microfluidic device. In the simple model, the minimum b_{in} for every particle is set to be zero when the center of the particle is positioned and aligned with the center of the obstacle. However, inside the microfluidic channel, the minimum b_{in} for every particle cannot be zero because the restriction of top wall as well as individual particle size will set a minimum b_{in} for that specific particle. We suspect that the minimum b_{in} for every particle we collected is close to the radius of the particle. In other words, particles only move along the channel wall where their minimum $b_{in} \geq a$. This restriction also means that b_{in} is very close to b_c already. Therefore, we only observe the scenario where $b_{in} > b_c$, which represent that the particle trajectory will always remain symmetric. (shown in Figure 5)

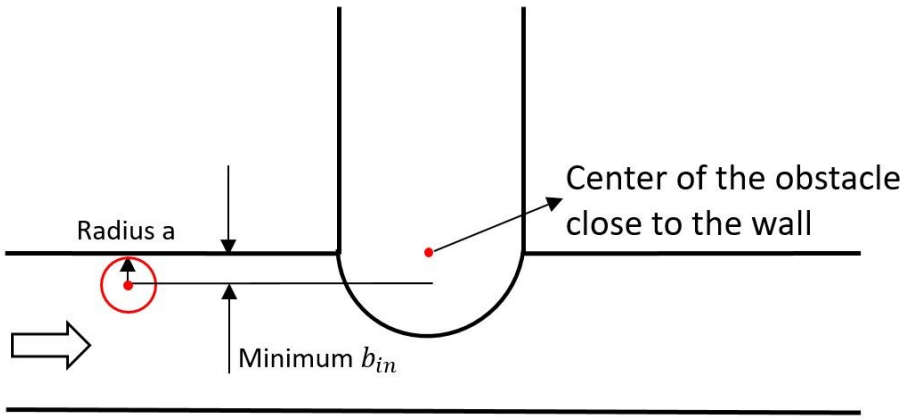

Figure 5. Schematic illustration for restriction of minimum bin for an individual particle with radius a due to top wall effect.

To further investigate our explanation for the wall effect, we normalize the outgoing offset (b_{out}) and particle radius (a) both with the obstacle radius (R) for each particle. The normalized b_{out} is plotted against normalized particle radius shown in Figure 6. We should recognize when a fluid obstacle is large enough (central angle is more than 180°), the center of obstacle shifts downward for all impact factor measurements. This vertical shift makes our impact factor to have a negative value of b_{in} and b_{out}. As mentioned earlier the meniscus of bubble is unlikely to be a perfect cylinder at the top and bottom of the fluid obstacle. Particles interacted with those parts are not qualified to be characterized by the particle-obstacle model. Thus, those data we collect should be eliminated. We observed that all symbols (only particles interacting with cylindrical part of obstacle) fall above the asymptotic line ($b_{out} = a$), representing $b_{out} \geq a$. Since $b_{out} = b_{in}$ is what we observe experimentally, then $b_{in} \geq a$ leads to $b_{in} > b_c$ where particle trajectory will always remain symmetry.

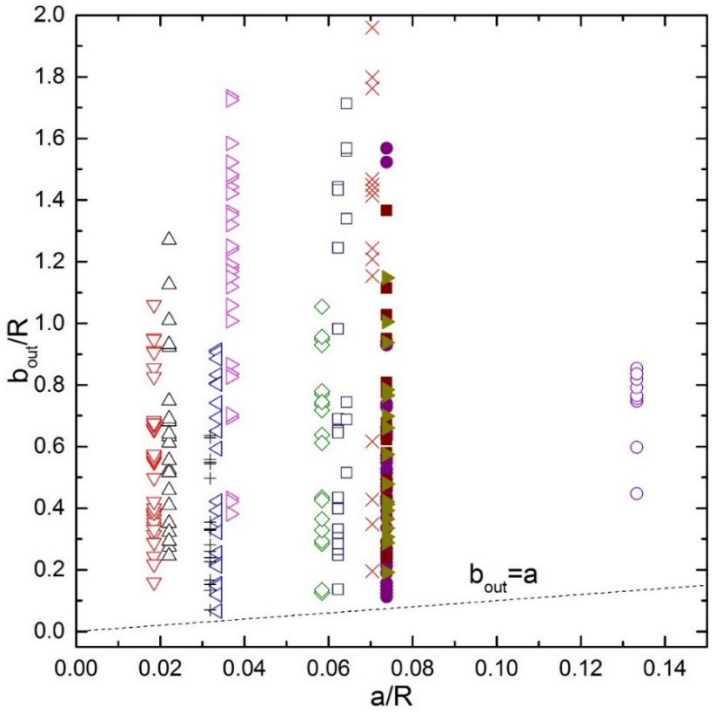

Figure 6. Outgoing offset (b_{out}) as a function of the particle radius (a), both normalized with the obstacle radius (R) for polystyrene particles in pressure-driven flow. The obstacle type and particle radius (a in μm) in the figure are: (△), H=100, G=4.4, a=1.5; (▽), H=100, G=31.2, a=1.5; (◁) , H=100 , G=13, a=2.5; (▷), H=100, G=13, a=2.5; (◇), H=100, G=30,a=4.5; (□) ,H=100,G=10,a=4.5; (○), H=100, G=6,a=10; (●) H=100, G=40,a=4.5; (■), H=100, G=30,a=4.5; (►) H=100, G=20,a=4.5; (+), H=33, G=47, a=1.5; (×), H=33, G=113, a=2.5.

1.3.3 Particle trajectories under gravity-driven flow

The trajectories of silica particles driven by gravity is characterized as particles move past either a solid or fluid obstacle. For a given particle size and obstacle radius, we measure incoming offset (b_{in}) and outgoing offset (b_{out}) of each trajectory. In contrast to pressure-driven flow, the result is similar to the macroscopic gravity driven pinched-flow–fraction (PFF)[14] study where asymmetric trajectories and size-based separation are observed due to hard-core particle- obstacle repulsion.

We observe both hydrodynamic (blue symmetric trajectories in Figure 8) and non-hydrodynamic touching collisions (yellow asymmetric trajectories in Figure 8) for both solid and fluid obstacles. The critical offset (b_c) is derived by averaging all b_{out} that are smaller than the transitioning point where "$b_{in} = b_{out}$" (horizontal dash line in Figure 12). The data points in plateau area are considered irreversible collisions, which occur when $b_{in} < b_c$. All trajectories with $b_{in} < b_c$ are asymmetric. The data points on the asymptotic line "$b_{in} = b_{out}$" (slope=1) describe reversible collisions, which occur when $b_{in} \geq b_c$. We also observe that the critical offset (b_c) for a given particle size around a solid obstacle is always greater than that of fluid obstacle (hollow symbols are all below the solid symbols in Fig. 12), for a given obstacle radius(R), particle radius (a) and gap (G).

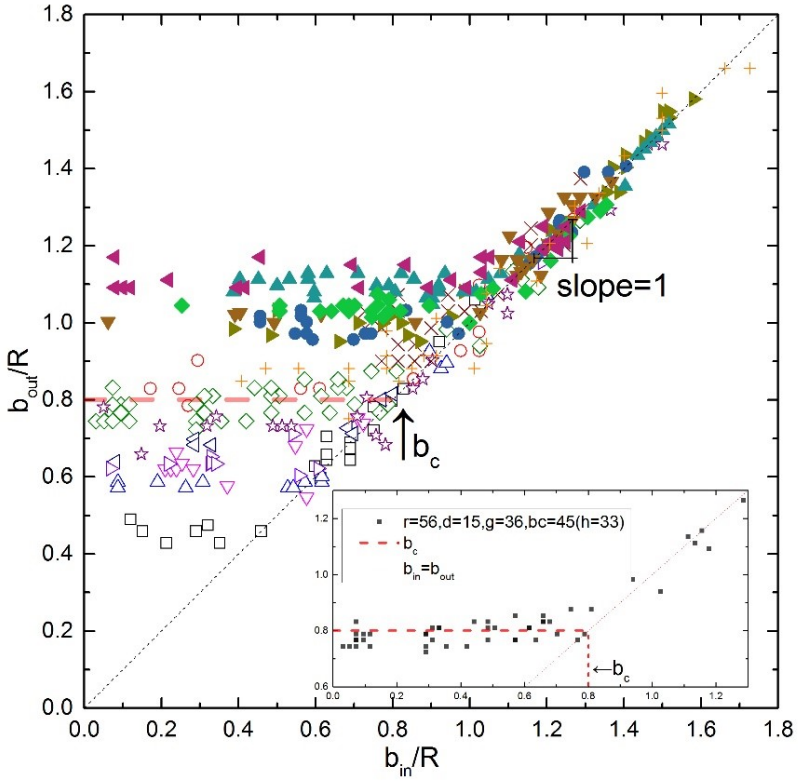

Figure 7. Scaling of outgoing offset (b_{out}) and incoming offset (b_{in}) with the obstacle radius(R) for silica particles with various radius (a) driven by gravity force. Solid symbols indicate solid obstacle while hollow symbols indicate fluid obstacle. The inset shows an example on how bc is clarified. The gaps (G in μm) and particle radius (a in μm) in the figure are: (□), R=65, a=5, G=34, b_c=34; (○), R=54, a=5, G=40, b_c=41; (△), R=68, a=7.5, G=36, b_c=46; (▽),R=68, a=7.5, G=32, b_c=50; (◇), R=56, a=7.5, G=36, b_c=45; (◁), R=68, a=10, G=36, b_c=53; (▷), R=65, a=10, G=38, b_c=48; (☆), R=54, a=10, G=47, b_c=47; (×), R=33, a=10, G=24, b_c=32; (+), R=33, a=5, G=24, b_c=29; (▼), R=63, a=5, G=27, b_c=61; (●), R=64, a=7.5, G=38,b_c=63; (▲), R=62, a=10, G=38, b_c=68; (▶), R=62, a=5, G=38, b_c=61; (◆), R=62, a=7.5, G=25, b_c=65; (◀), R=63, a=10, G=27, b_c=69.

Not only a critical offset (b_c) is observed for all particles around obstacles, but we also observe size-based separation in our microfluidic system. Flowing mixtures of different sizes of particle in the channel, the particles would flow around the same obstacle (same radius(R) and gap (G)). In this case, larger particles show larger outgoing offset (b_{out}) and

consequently greater critical offsets (b_c) (see different particles' b_c in caption of Figure 12 and trajectories of 10μm and 20 μm silica particles in Figure 12). When particles have touching collisions with obstacle, the center of a larger particle is more distant from the obstacle center than smaller ones, thus the outgoing offset (b_{out}) is larger.

To further investigate the size-based separation behavior of particles in the microfluidic system, we show the non-dimensional critical offset as a function of non-dimensional particle radius in Figure 13. When different sizes of particles pass around the same obstacle, b_c increases linearly with radius of particles. This linear relationship has also been discovered in previous macroscopic studies[6, 7]. The critical offset (b_c) for solid obstacle is always greater than the b_c for fluid obstacle shown in Figure 13 with hollow symbols that are all below the solid symbols in the small a/R regime.

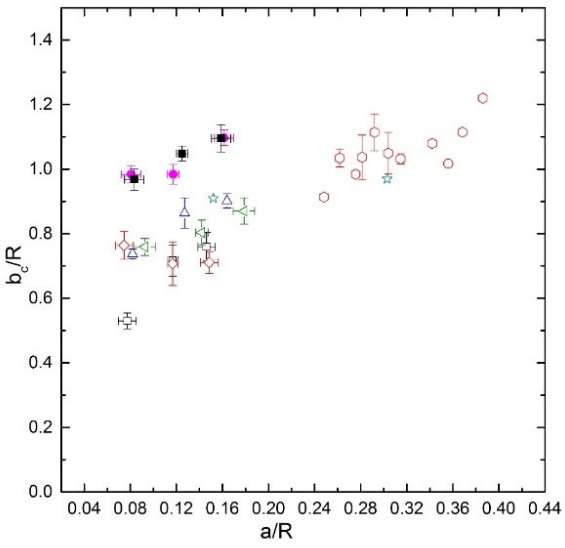

Figure 8. Scaling of critical offset (b_c) and particle radius (a) with the obstacle radius(R) for silica particles. The gaps (G in μm) and particle radius (a in μm) in the figure are: (□), g=35, R=68;(○), g=25, R=68; (△), g=27, R=61; (◇) g=50, R=68; (◁),g=40, R=55; (☆) g=25, R=33; (●), g=38, R=62; (■) g=27, R=62

Due to the slight uncertainty error occurred in microfabrication, the PDMS-made solid obstacle has more roughness than the fluid obstacle. The effect of surface roughness can reduce the pull-off force between particle and obstacle[17,18] Surface roughness balances the hydrodynamic restraining torque acting on the particles to obstacle surface. As a result, more net pull-off force is required for silica particles to leave from the smoother fluid obstacle surface than from the rougher PDMS surface. This larger restrain causes the extension of particle trajectory on surface, and leads to smaller outgoing offset (b_{out}) and critical offset (b_c). The deformation of bubble due to any vibration in experiments (e.g. when tilt the microscope), air tightness of microfluidic system and particle interaction with fluid obstacle, however, create more noise/scattered data point in fluid data than those of in solid ones. We believe decreasing the surface roughness of microchannel in design and fabrication step, as well as the robustness of setup in experimental step, would eliminate some noise from our measurements.

1.4 Conclusion

For the first time, we have used a simple model particle-obstacle collision for the force-driven DLD to investigate difference between particle separation at both SWI and AWI, and to compare active(pressure-driven) and passive (gravity driven) Deterministic Lateral Displacement. We developed novel microfluidic-based platforms with semi-circular cylinder solid (PDMS) and fluid (bubble) obstacle in PDMS microchannel to monitor colloidal transport with negligible Reynolds numbers (Re $<<1$) in real time. The particle-obstacle interaction take place when suspended spherical particle passing through a constriction between a fixed half-circular cylindrical obstacle and a plane during our

experiments. The simple model with three important parameters (b_{in}, b_{out} and b_c) allow us to characterize two types of collision with corresponding trajectories: purely hydrodynamic ones with for-and-aft symmetry and non-hydrodynamic touching collision with asymmetric trajectory. We found that particles exhibit no net lateral displacement and show symmetric trajectories for both solid and fluid obstacles in a flow-driven case. We have discussed that the range of b_{in} for particles is limited by the restriction of the top wall, causing particles to go around obstacle only in a symmetric trajectory. Only in a case where the constriction created by the bubble is larger enough, the particle will go in an asymmetric trajectory due to pinched flow effect that is comparable to what Mingxiang and others have founded in PFF system. On the other hand, we have found that there is a clear particle separation scheme in gravity-driven flow experiment where particles experience asymmetric trajectories. This result is in an agreement with most of DLD and simple model macro and microscopic system. We observe that the critical offset increases with increasing particle radius in the presence of the non-hydrodynamic interactions, which coincides with the previous macroscopic studies[16].Given similar obstacle radius(R), particle radius (a) and gap (G), the critical offset (b_c) of particles around solid obstacle is bigger than that of bubble. Specifically, we have found that magnitude of b_c from solid obstacle (b_{cs}) is greater than that of fluid obstacle (b_{cf}), suggesting that fluid obstacle is less efficient in particle separation. In essence, b_c is present in gravity driven cases but not in flow driven cases. b_c increases with particle size for both solid obstacle and bubble. b_c from solid obstacle is greater than that of fluid obstacle. ($b_{cf} < b_{cs}$). Future work can focus more on the particle-bubble collision event that have been highlighted by group of flotation experts where they look at particle-bubble absorption attachment and detachment efficiency and

probability. The work can also extend into area of environmental issue to remove contaminant or toxic particulate from groundwater to improve better water resource.

2. Particle deposition near fluid interfaces

2.1 Introduction

Metamaterials are a fast-growing area of research interest where materials are engineered to have emergent properties by assembling multiple elements in repeating patterns in nanoscales[19]. The concept of metamaterials can be found in nature as well. For example, beetle wings are composed of repeating patterns of concentric rings. The hierarchical structures of concentric rings found give rise to the beautiful color to wings that serve as their protective coloration[20]. Another example is butterfly wings showing triangular hole patterns at nanoscale that ultimately give rise to its iridescent color[21]. Our proposed nanomanufacturing of metamaterials scheme is applied to solve current continuous manufacturing barrier where current large scaled printed electronics based on colloidal inks will not work for most metamaterial applications, because metamaterials require the materials to be controlled from nano-scale dimensions to micro structures to manufacture materials[2223]. Continuous manufacturing of hierarchical assembled material over a large area is another challenge current technology needed to overcome and reduce cost[24]. To construct tunable metamaterials, structures must be controlled from nanoscales. Therefore, we propose a solution to manufacture hierarchical materials by rapidly transporting Nps loaded droplets onto pre-define physicochemical patterns initially followed by self-directed assembly of particle microstructures via mediated interaction. Lastly rapid immobilization of local and global hierarchical structures through in situ polymerizable media will produce a new hierarchical structure which will have new emergent properties, hence a new metamaterial.

2.2 Materials & Methods

Octadecyltrichlorosilane (OTS) for substrate patterning, Trimethylolpropane Ethoxylate Triacrylate (ETPTA) as photocurable oil and 2-Hydroxy-2-methylpropiophenone (Darocur 1173) as photoinitiator are purchased Sigma-Aldrich (St. Louis, MO). Trichloro perfluorooctyl silane is purchased from Sigma-Aldrich for salinization. Silica particles (diameter = 1, 0.5μm) are purchased from Bang's Laboratories (Fishers, IN). Fluorescent silica particles (dimeter = 1, 0.5μm) are purchased from MicroMod Partikeltechnologie GmbH (Germany). Iron Oxide coated magnetic particles (diameter=1, 0.5 μm) are purchased from microparticles GmbH (Germany). 35mm in diameter petri dish is purchased from Thermo Fisher Scientific Inc. (Pittsburg, PA). All products are used as received.

2.2.1 Microfabrication

Molds for the master PDMS stamp for microcontact patterning are fabricated using standard soft photolithography method. A double layer coating process of SU-2025 on wafers is used to ensure feature adhesion to wafers after developing. After creating wells of desired dimension, a salinization process is introduced to make features more resistant for PDMS to be peeled off from the molds. Figure 9 is the final confocal images of the master PMDS stamp ready to be used for microcontact patterning.

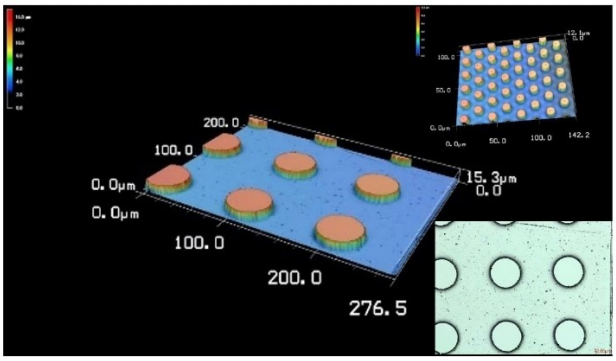

Figure 9. 3D optical confocal microscopic image of the PMDS master stamp

2.2.2 Surface Characterization

We use microcontact patterning (μCP) technique to prepare our samples[7,25,26]. The substrate glass coverslips were patterned to have alternating regions of hydrophobic circles (OTS) and hydrophilic regions (clean glass surface). μCP methods has been widely used to functionalized surfaces for self-assembly molecules such as using thiol, a silane based molecule by Whiteside's group[25]. μCP methods allows SAM groups to be oriented closely and packed perpendicular to the surface uniformly, which results in a high quality of the thin film[26].

Microcontact patterning

Patterned coverslip glass substrates with a heterogenous surfaces were prepared by micro-contact printing[27]. First, to complete creating a dust-free glass, a glass coverslip is rinsed with IPA and acetone, then is placed on a 200°C to remove excess moisture. The OTS ink with 6 mM[28] in toluene is deposited onto the stamp and dried in a flow of nitrogen

gas for a few seconds. Then for 1 min at 70 °C, the stamp was brought into contact with the glass substrate, which was pretreated under oxygen plasma for 2 minutes. After release of the stamp, the glass was rinsed with acetone.

2.2.3 Particle/Oil Solution Preparation

1-Octadecanol Coated Silica Particle

The coating procedure is followed by R. Beckham thesis where the particles must have a silica exterior to work[29]. This coating reaction was initially published using a terminal alkane-acid, but a terminal alkane-alcohol can be used alternatively.1-octadecanol is also known as stearyl alcohol where the -OH group on silica particles reacts with the alcohol group. First, adding 200 μL of silica particles to 1 mL of DI water followed by centrifuging and redispersing in deionized water for five times, then in 200 proof ethanol for at least five times. In fume hood, make a 10-mL solution with 1-mL of particle and 9-mL 200 proof ethanol placed in flask. Add 2 pellet of octadecanol into the solution and maintain temperature at 150 ºC for 4 hours to allow ethanol to evaporate and to allow octadecanol to fixate to particles. Chloroform is used to remove unreacted octodecanol. The final octadecanol coated silica particle should have little net charge between 0 to 5 mV and must be kept in ethanol to prevent aggregation.

ETPTA Oil/Silica Particle Preparation

Coated or Uncoated silica particles first are to be cleaned and rinsed with deionized water and redispersed in ethanol for at least three times to remove unwanted salt group or contaminates. Silica particles have similar refractive index that matches with ethanol[7]. A careful cleaning process must be addressed not to remove ethanol with particles altogether.

ETPTA Oil is then added into the cleaned particle solution with some ethanol. Since ethanol and ETPTA Oil are immiscible, a 70 ºC heating in oven over night will ensure all the leftover ethanol evaporate. A 30-minute sonication after heating will make particles monodisperse in ETPTA oil solution ready for drop deposition.

2.3 Experimental Setups

Figure 10 shows a schematic illustration of the dynamic particle oil deposition process to create droplets confined in patterned surfaces. The ETPTA oil drop with particles are deposited onto the pattered coverslip that is placed in a 35-mm in diameter small petri dish. Then a rinsing process by deionized water is taken place to immerse the particle droplets in DI-water. A Zeiss inverted confocal microscope is used to image the final particle droplets confined on pre-pattern surfaces.

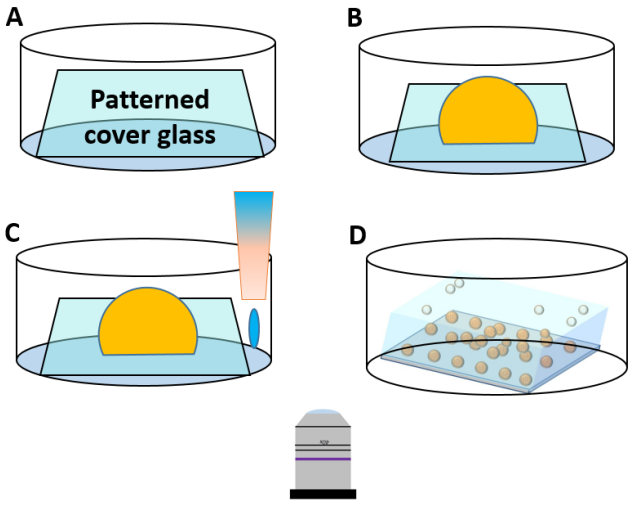

Figure 10. an illustration of the experimental system setup. (A)First place the patterned cells into petri dish. (B) then deposit an ETPTA drop with Nps (C) quickly followed by DI water rinsing to create (D) desirable hierarchical assembly.

2.3.1 UV-Light Polymerization

The ETPTA-Particles solution has 5 percent by volume of photoinitiator (Darcur 115), which absorb the UV light and turn the free radical energy into initiating chemical reaction. The samples are placed onto the UV-plates by UVP benchtop 3 UV transilluminator (Upland, CA) for 6 minutes. Then the water is removed from the sample and the photonic dome feature with particles are observed similar to the ones found in Kim, et. al group[7,30]

2.4 Result & Discussion

The section summarizes the result of our oil deposition near fluid interface with different microscopy images. The samples under bright-field confocal microscope show that 1. the deposition of plain ETPTA oil droplets onto the surfaces. With different geometric arrangement of the master PMDS stamps, desired shape and size of micro contact patterning can be achieved. 2. The deposition of different types of nanoparticles with ETPTA oil droplets onto the surfaces shows Brownian particle movement inside the drop. 3. The oil droplets confined on patterns are relatively stable over time resisting shear force from the surrounding. 4. Fluorescent imaging shows the distribution of particles inside the drops as most of the particle eventually will be displaced on the triple contact line (oil water surface interfaces). 5. Polymerization of oil or oil with particle feature on surfaces are imaged with electron optical microscope as well as Scanning Electron Microscope to analyze surface topology profile.

2.4.1 Surface energy requirement for heterogenous surfaces

The goal is to characterize physicochemical surface that will not only limit drop deposition to the pre-patterned region thermodynamically, but also provide strong non-

equilibrium pinning force for drop to sit so that they can resist shear forces from the bulk phase surrounding. The wetting properties of the surfaces thus are important to dictate if the surfaces are hydrophobic/oleophilic with respect to hydrophilic/oleophobic surroundings[31,32].

2.4.2 Young's Equation

We use Young's Equation by means of contact angle measurement to determine the surface energy thermodynamically for ideal oil drop deposition. In Young's equation, the force balance (contact angle, surface tension and interfacial tension) comes to an equilibrium where the oil drop interface intersect with the solid interface. The energy requirements as well as wettability of the surface are illustrated in Figure 11 using contact angle measurements. In Figure 11A, hydrophobic/oleophilic surface in in air will favor the oil deposition in a water medium. For a surface that is hydrophilic in air will prevent oil deposition in a water medium shown in Figure 11B.

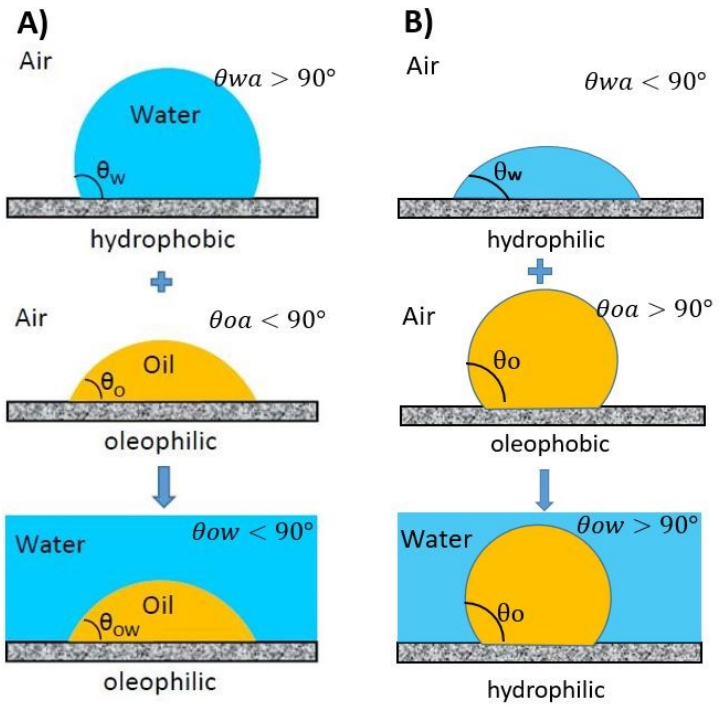

Figure 11. Surface energy requirements for desirable oil wetting properties. In case (A) a hydrophobic/oleophilic surface in air will result a olephilic surface in water. Surfaces that are hydrophilic in air will prevent the deposition of the oil drops.

In the case of OTS-pattern surfaces, contact angles of water and ETPTA oil in air are about 110 ° and 55° respectively using our contact angle machinery shown in Figure 12. By using Young's equation for modeling various surfaces derived in Bhushan et. al, the contact angle of the ETPTA oil drop in water can be theoretically estimate if the surface is oleophilic under water[31].

$$\cos\theta ow = \frac{\Upsilon oa \ \cos\theta o - \Upsilon wa \cos\theta w}{\Upsilon ow} \quad (1)$$

by plugging in surface tension value for both ETPTA/Water in equation (1), ETPTA oil, the contact angle is estimated < 90°, indicating the ETPTA oil drop is likely to be wetted onto OTS-patterned surfaces in water.

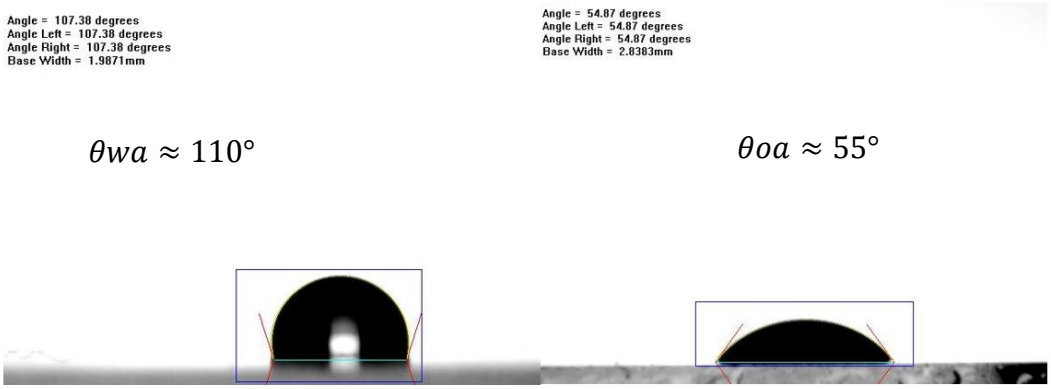

Figure 12. Experimental measurements of contact angles using a contact angle machinery. A OTS coated surfaces are measured $\theta wa \approx 110°$ and $\theta oa \approx 55°$.

2.4.3 ETPTA on patterned surfaces

After depositing oil drop in the water medium, a dome-shape pattern formed on the patterned surfaces over a large area. The Figure 13A and 13B on the top are the close-up views of larger patterned areas shown in 13C and 13D. Notice that the 13A and 13C are patterned with 20 X 20 um stamp whereas 13B and 13D are printed with a 50 X 50 um stamp. The accuracy and precision of OTS-micro contact patterns are shown to create the surfaces for ETPTA oil to selectively deposited onto the designated regions.

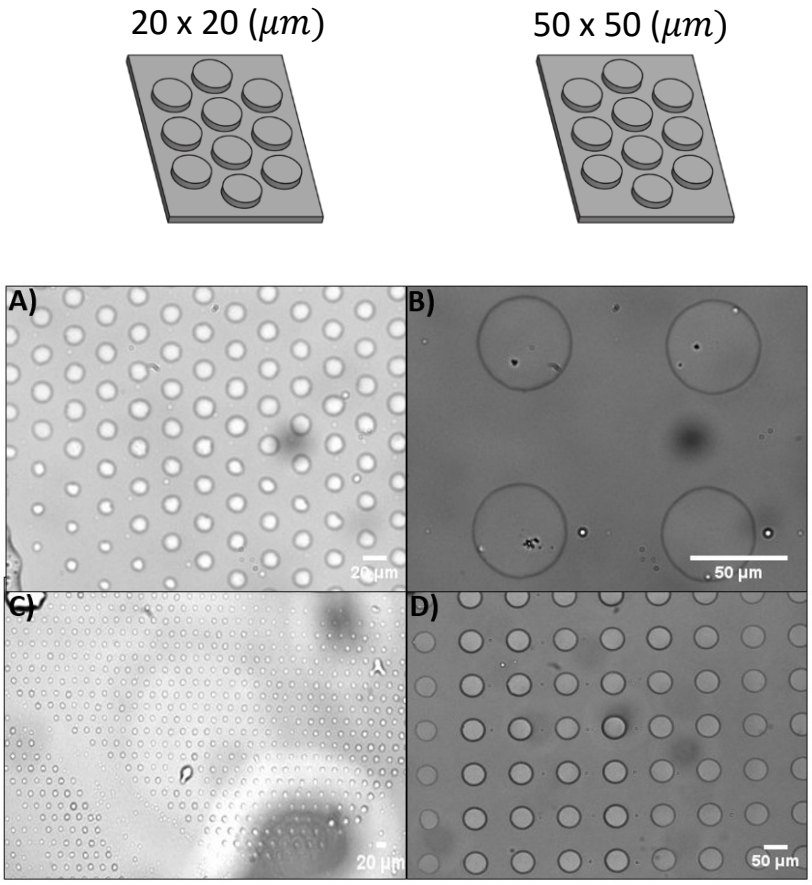

Figure 13. Images of ETPTA patterned surfaces corresponding to different geometric PDMS stamp. (A) and (B) are the close-up view of patterned region (C) and (D).

2.4.4 ETPTA with silica particles

Figure 14A shows the areas after deposition of ETPTA-particle drops. Most of the particles are well suited inside the drop with few left on the surroundings. Figure 14B shows a more detailed view of the particle distribution. The presence of the particles tends to deform oil droplet shape on pattern. Over time particle are slowing sliding from top of the droplets down to the bottom of pattern. We also notice particles are more likely to be positioned at the triple contact line. (Water-Oil-Surface interfaces)

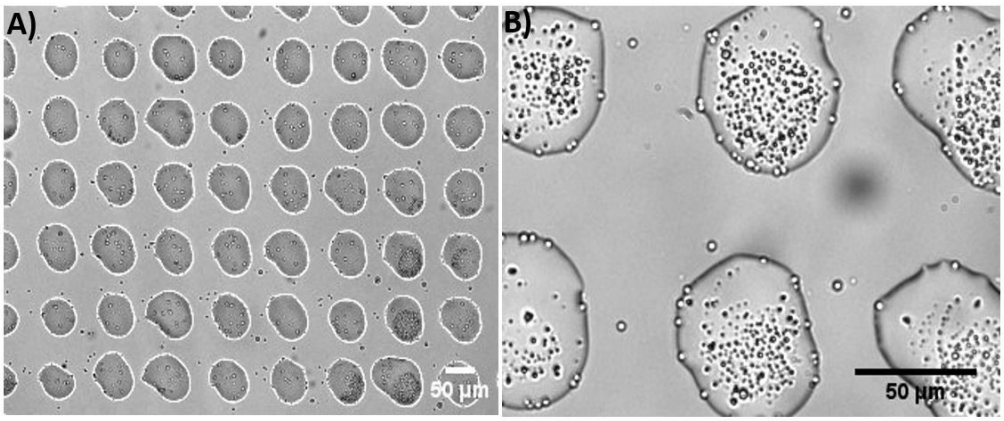

Figure 14. Images of ETPTA with silica Nps on patterned surfaces.

2.4.5 ETPTA with 1-Octadecanol coated silica particle

1-Octadecanol has an alcohol group that esterifies with the -OH group on silica particles, which makes the particles very hydrophobic[29]. Hydrophobic coated silica particles will more easily dispersed in the ETPTA-Oil phase. Hydrophobicity of the particle also helps prevent particles from sticking onto both OTS treated and untreated regions. Under confocal imaging, we observe Brownian particle motions within the drop.

2.4.6 ETPTA with fluorescent silica particle

Fluorescent silica particles (dimeter = 1, 0.5µm) are purchased from MicroMod Partikeltechnologie GmbH, which has excitation wavelength of 485 nm and emission wavelength of 510 nm. Under the fluorescent confocal microscope, the result confirms with our observation on plain silica-ETPTA system where the particles are position around the triple contact line over time and particles are truly confined within the pattern area inside

oil drops. In Figure 15, the image show deposition of 1 μm fluorescent silica particles on the top. The bottom picture shows a 3D scan stacking of particle position within the drops.

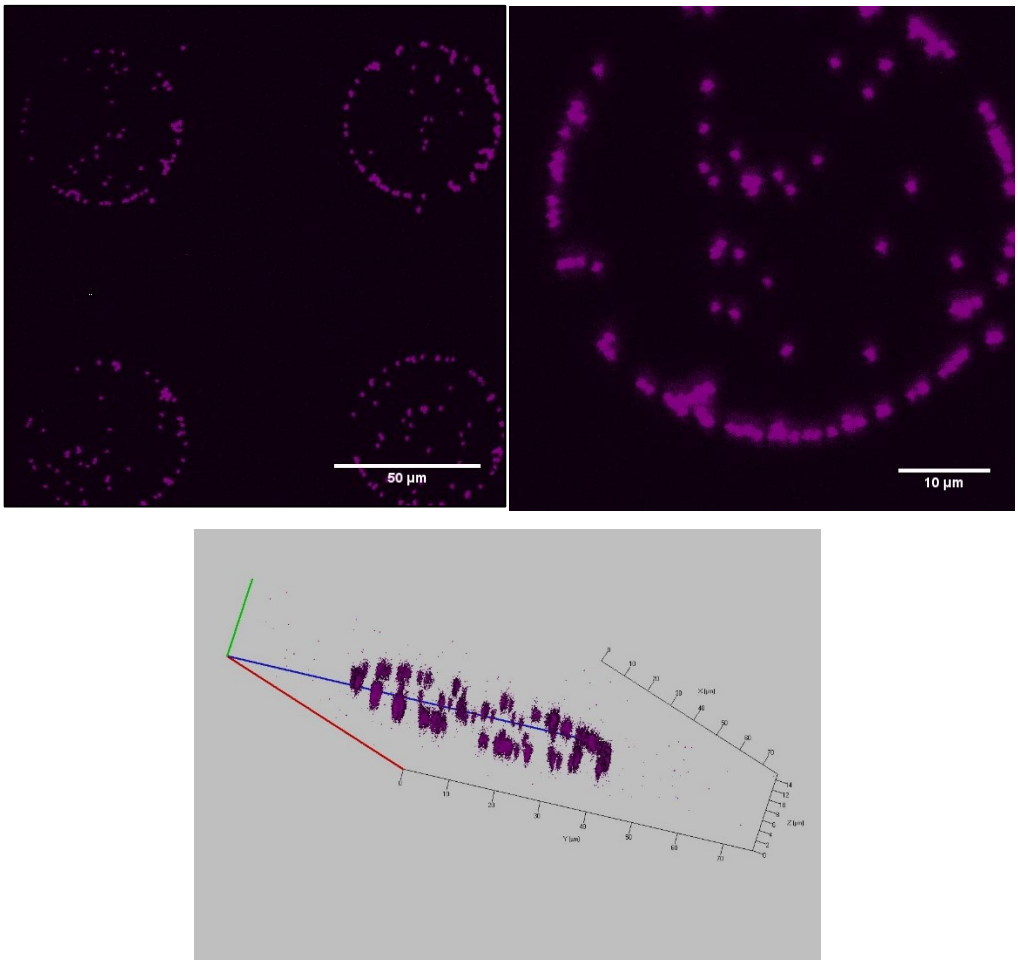

Figure 15. Confocal images of ETPTA with florescent silica Nps on patterned surfaces. The pink color of particle intensity signals is from post processing with the Ziess zen microscope software. The image at the bottom is the z-stacks of fluorescent silica particle 3D scans for particle distribution.

2.4.7 Stability of ETPTA oil droplets confined in pattern

The oil droplets confined on patterns are relatively stable over time resisting shear force from the surrounding shown in Figure 16.

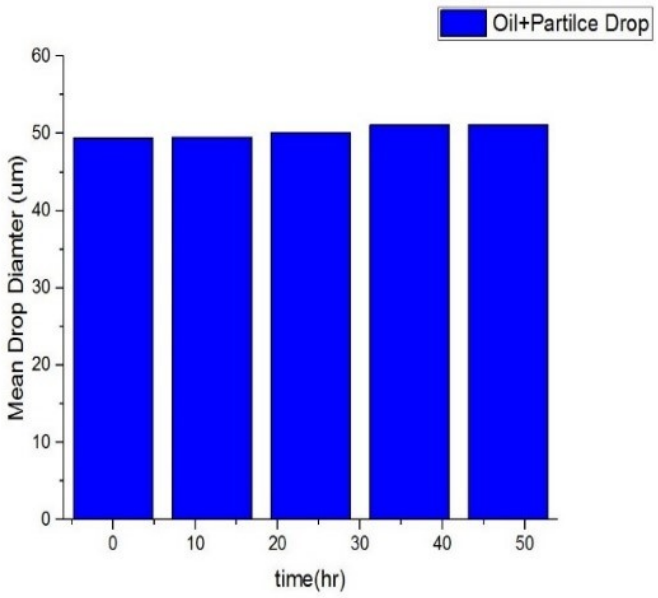

Figure 16. stability analysis of mean drop diameters of ETPTA with silica particle over time.

2.4.8 Polymerization

Polymerization of oil or oil with particle feature on surfaces are imaged with electron optical microscope as well as scanning electron microscope to analyze the surface topology profile.

Electron Confocal Microscope

The Nikon confocal microscope uses UV-Laser light to detect surface profile of polymerized solid domes shown in Figure 17. The surface profile analysis shows the average height of the spherical cap feature are about 6 μm. The diameters of the patterned photonic domes are in average of 51-μm in diameter, which shows the feasibility of UV polymerization technique to capture global hierarchical nanostructures.

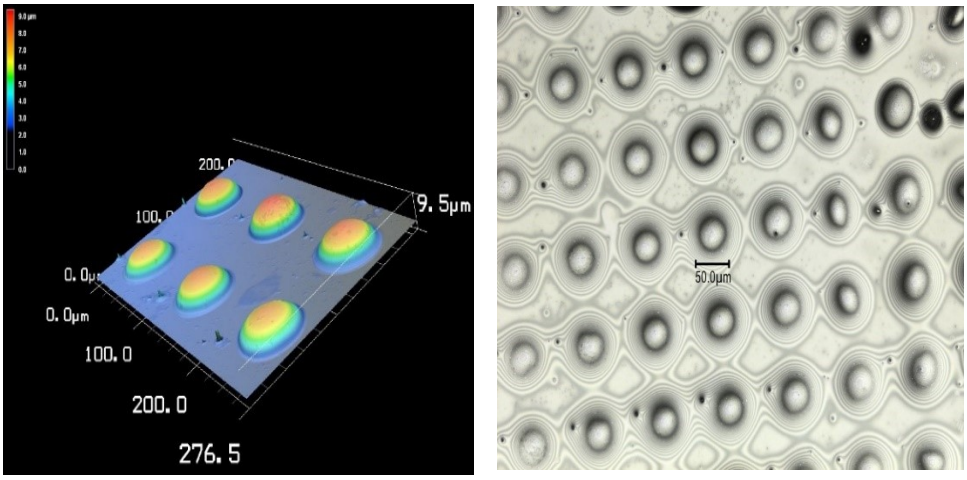

Figure 17. Confocal images of electronic and optical scans of polymerized oil/particle features.

Scanning Electron Microscope

The SEM micrographs of polymerized ETPTA/Nps feature are acquired using a FEI Quanta 200 ESEM. The sample of our polymerized feature on glass coverslip is first coated with silver (by using low vacuum sputtering coating) to have an electronically conductive surface. The standard operating condition of SEM is under a high vacuum with sample tilted about 15° to enhance topological contrast. The polymerized drops with 1 um silica particles are imaged with SEM in Figure 18**.** Figure 18 on the left shows orderly array of polymerized structures. When zooming in for a higher resolution, we observe particles protruding out of the domes surfaces on the right. The success of immobilization of particles within oil drops are clearly presented.

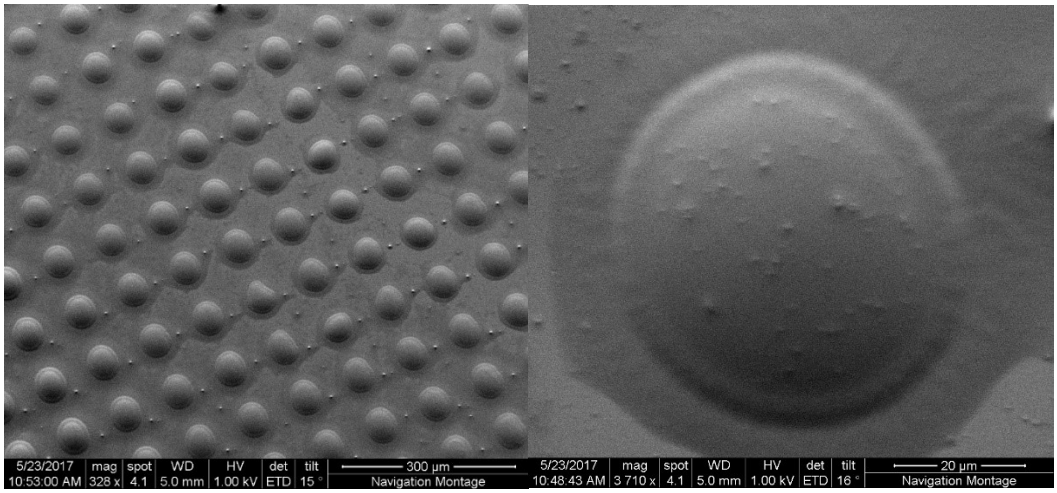

Figure 18. SEM images of Polymerized ETPTA with silica Nps on patterned surfaces.

2.5 Conclusion

We successfully designed a pre-defined heterogenous physiochemical surfaces to confine the deposition of oil-particle drop (ETPTA+silica) to study the strength of colloidal self-assembly over a large area. We demonstrate that we can selectively deposit the oil drops with Nps on to the hydrophobic patches, and Nps are remained mostly within the drops during the process. By analyzing through fluorescent silica particle under confocal as well as bright field microscope, we can observe particles' Brownian motion and their movement near fluid interfaces. We achieve rapid immobilization of local and global hierarchical structures through in situ polymerizable media. There are more rooms for future works to investigate into the art of particle reconfiguration within oil drop. The future applications can further expand into investigating biological applications such as morphogenesis where biological formations at many levels can achieve higher order of multicellular organisms. Overall, the established method of constructing metamaterials will enable us solve many more complex engineering problems ahead.

3. Reference

1. Huang, L. R., Cox, E. C., Austin, R. H. & Sturm, J. C. Lateral Displacement. **304,** 987–991 (2004).
2. Liu, Z. *et al.* Rapid isolation of cancer cells using microfluidic deterministic lateral displacement structure. *Biomicrofluidics* **7,** 1–10 (2013).
3. Risbud, S. R. Particle-Obstacle Interactions At Low Reynolds Number: Implications For Microfluidic Applications. (2013).
4. Risbud, S. R., Luo, M., Fréchette, J. & Drazer, G. Analysis of the trajectory of a sphere moving through a geometric constriction Analysis of the trajectory of a sphere moving through. **62001,** (2013).
5. Ralston, J., Fornasiero, D. & Hayes, R. Bubble-particle attachment and detachment in flotation. *Int. J. Miner. Process.* **56,** 133–164 (1999).
6. Wang, W., Zhou, Z., Nandakumar, K., Xu, Z. & Masliyah, J. H. Attachment of individual particles to a stationary air bubble in model systems. *Int. J. Miner. Process.* **68,** 47–69 (2003).
7. Kim, S. H., Yi, G. R., Kim, K. H. & Yang, S. M. Photocurable pickering emulsion for colloidal particles with structural complexity. *Langmuir* **24,** 2365–2371 (2008).
8. Zhou, J., Ellis, A. V. & Voelcker, N. H. Recent developments in PDMS surface modification for microfluidic devices. *Electrophoresis* **31,** 2–16 (2010).
9. Zhou, R. & Wang, C. Acoustic bubble enhanced pinched flow fractionation for microparticle separation. *J. Micromechanics Microengineering* **25,** 84005 (2015).
10. Garstecki, P., Fuerstman, M. J., Stone, H. a & Whitesides, G. M. Formation of droplets and bubbles in a microfluidic T-junction-scaling and mechanism of break-

up. *Lab Chip* **6,** 437–446 (2006).

11. Balvin, M., Sohn, E., Iracki, T., Drazer, G. & Frechette, J. Directional locking and the role of irreversible interactions in deterministic hydrodynamics separations in microfluidic Devices. *Phys. Rev. Lett.* **103,** 2–5 (2009).
12. Frechette, J. & Drazer, G. Directional locking and deterministic separation in periodic arrays. *J. Fluid Mech.* **627,** 379–401 (2009).
13. Du, S. & Drazer, G. Deterministic separation of suspended particles in a reconfigurable obstacle array. *J. Micromechanics Microengineering* **114002,** 114002
14. Luo, M., Sweeney, F., Risbud, S. R., Drazer, G. & Frechette, J. Irreversibility and pinching in deterministic particle separation. *Appl. Phys. Lett.* **99,** 2009–2012 (2011).
15. Frechette, J. & Drazer, G. Directional locking and deterministic separation in periodic arrays. *J. Fluid Mech.* **627,** 379–401 (2009).
16. Bowman, T., Frechette, J. & Drazer, G. Force driven separation of drops by deterministic lateral displacement. *Lab Chip* **12,** 2903 (2012).
17. Das, S. K., Schechter, R. S. & Sharma, M. M. The Role of Surface Roughness and Contact Deformation on the Hydrodynamic Detachment of Particles from Surfaces. *Journal of Colloid and Interface Science* **164,** 63–77 (1994).
18. Cheng, W., Dunn, P. F. & Brach, R. M. Surface Roughness Effects on Microparticle Adhesion. *J. Adhes.* **78,** 929–965 (2002).
19. Schurig, D. *et al.* Metamaterial Electromagnetic Cloak at Microwave Frequencies. *Science (80-.).* **314,** 977–980 (2006).

20. Sharma, V., Crne, M., Park, J. O. & Srinivasarao, M. Structural Origin of Circularly Polarized Iridescence in Jeweled Beetles. *Science (80-.).* **325,** 449–451 (2009).

21. Biró, L. P. & Vigneron, J. P. Photonic nanoarchitectures in butterflies and beetles: Valuable sources for bioinspiration. *Laser Photonics Rev.* **5,** 27–51 (2011).

22. Performances, L. I. Importance of Monomer Interfacial Tension For UV Curable Litho Inks Performances. 1–8 (2016).

23. Biancaniello, P. L., Kim, A. J. & Crocker, J. C. Colloidal interactions and self-assembly using DNA hybridization. *Phys. Rev. Lett.* **94,** 94–97 (2005).

24. Muangnapoh, T., Weldon, A. L. & Gilchrist, J. F. Enhanced colloidal monolayer assembly via vibration-assisted convective deposition. *Appl. Phys. Lett.* **103,** (2013).

25. Mrksich, M. & Whitesides, G. M. Patterning self-assembled monolayers using microcontact printing: A new technology for biosensors? *Trends Biotechnol.* **13,** 228–235 (1995).

26. Quist, A. P., Pavlovic, E. & Oscarsson, S. Recent advances in microcontact printing. *Anal. Bioanal. Chem.* **381,** 591–600 (2005).

27. Kim, S. H., Kim, S. H. & Yang, S. M. Patterned polymeric domes with 3D and 2D embedded colloidal crystals using photocurable emulsion droplets. *Adv. Mater.* **21,** 1–6 (2009).

28. JEON, N. L., Finnie, K., Branshaw, K. & NUZZO, R. G. Structure and stability of patterned self-assembled films of octadecyltrichlorosilane formed by contact printing. *Langmuir* **13,** 3382–3391 (1997).

29. Lu, M., Bevan, M. A. & Ford, D. M. Interfacial colloidal sedimentation equilibrium. II. Closure-based density functional theory. *J. Chem. Phys.* **127,** (2007).

30. Kim, S. H., Kim, S. H. & Yang, S. M. Patterned polymeric domes with 3D and 2D embedded colloidal crystals using photocurable emulsion droplets. *Adv. Mater.* **21,** 3771–3775 (2009).

31. Jung, Y. C. & Bhushan, B. Wetting behavior of water and oil droplets in three-phase interfaces for hydrophobicity/philicity and oleophobicity/philicity. *Langmuir* **25,** 14165–14173 (2009).

32. Shen, L. & Zhu, J. Heterogeneous surfaces to repel proteins. *Adv. Colloid Interface Sci.* **228,** 40–54 (2016).

VITA

LEO (TSUNG-CHENG) FENG

116 West University Pkwy ♦ Baltimore, MD 21210 ♦ Phone: (443) 469-4599 ♦ tsungchengfeng@gmail.com

SUMMARY

- Strong nanotechnology, engineering background with exceptional problem solving, analytical, and interpretive skills evident from research laboratory experience at Johns Hopkins University
- Experienced in teamwork environment and was a project leader in a graduate research lab with strong communication and organizational skill.
- Great mentor and motivator by my experience as a Lab Teaching Assistant advising 20+ students
- Foreign Language: Mandarin Chinese
- Computer skills: JAVA, C++, Matlab, Apsen, Microsoft office, AutoCad, Labview, Comsol
- Research skills: Nanotechnology, Microfluidics, Photolithography, Chromatography, Distillation, Bioreactor

EDUCATION & TRAINING

Master of Science, Chemical & Biomolecular Engineering, Johns Hopkins University Expected Dec 2016

- Cumulative GPA: 3.61/4.00

Bachelor of Science, Chemical & Biomolecular Engineering, Johns Hopkins University May 2013

- Chemical & Biomolecular Engineering Excellence Award

RESEARCH&WORK EXPERIENCE

Graduate Researcher in Frechette Lab, Johns Hopkins University Jan 2016-present

- Independent research topic on interfacial phenomena of nanoparticles in microfluidics

Internship at Shenyang Haosong Ceramics Co., LTD, China June 2014- Sep 2014

- Performed particle ink analysis for ceramic tile in R&D department
- Pilot scale-up experiment
- Assisted Departmental Managers for meetings and conferences

Graduate Research Assistant in Leheny Lab, Johns Hopkins University June 2013-Sep 2013

- Led an independent project team in particle separation in Liquid Crystal medium
- Fabricated and optimized microfluidic devices for experiments

Physics Department Laboratory Teaching Assistant, Johns Hopkins University Sep. 2012-Dec 2012

- Managed teaching lab set ups and maintenance.
- Provided academics support for students

Undergraduate Research Assistant in Drazer Lab, Johns Hopkins University May. 2011- May 2013

- Researched particle delivery, migration and separation in biocompatible microfluidic device
- Performed experiment and data analysis to show distinctive particle separation and rheology under specifications

ACCOMPLISHMENT

Principal Technician for a Published Research Paper, Johns Hopkins University **Dec. 2012**

- *Force Driven Deterministic Lateral Displacement for Particle Separation in Microfluidic Devices*
  R. Devendra and G. Drazer, Anal. Chem. **84**, 10621 (2012)

Chemical & Biomolecular Engineering Excellence Award **March 2016**

- Recognized by the Chemical & Biomolecular Engineering department as an undergraduate student who stands out for academic performance, dedication to research, and service.